ROMP-based Glycopolymers with High Affinity for Mannose-Binding Lectins

Clément Gonnot, Mathieu Scalabrini, Benoit Roubinet, Célia Ziane, Fabien Boeda, David Deniaud, Ludovic Landemarre, Sébastien Gouin, Laurent Fontaine, Véronique Montembault

ROMP-based Glycopolymers with High Affinity for Mannose-Binding Lectins

Clément Gonnot[a], *Mathieu Scalabrini*[b], *Benoit Roubinet*[c], *Célia Ziane*[a], *Fabien Boeda*[a], *David Deniaud*[b], *Ludovic Landemarre*[c], *Sébastien G. Gouin*[b], *Laurent Fontaine*[a,*], *Véronique Montembault*[a,*]

[a] Institut des Molécules et Matériaux du Mans (IMMM), UMR 6283 CNRS – Le Mans Université, Avenue Olivier Messiaen, 72085 Le Mans Cedex 9, France

[b] Nantes Université, CNRS, CEISAM UMR 6230, F-44000 Nantes, France

[c] GLYcoDiag, 2 rue du Cristal, 45100 Orléans, France

KEYWORDS. ROMP, Azlactone, Glycopolymers, Multivalency, Inhibiting effect, Lectins

ABSTRACT. Well-defined, highly reactive poly(norbornenyl azlactone)s of controlled length (number-average degree of polymerization $\overline{DP_n}$ = 10 to 1,000) were made by ring-opening metathesis polymerization (ROMP) of pure *exo*-norbornenyl azlactone. These were converted into glycopolymers using a facile post-polymerization modification (PPM) strategy based on click aminolysis of azlactone side groups by amino-functionalized glycosides. Pegylated mannoside, heptyl-mannoside, and pegylated glucoside were used in the PPM. Binding inhibition of resulting glycopolymers was evaluated against a lectin panel (Bc2L-A, FimH, langerin, DC-SIGN, ConA). Inhibition profiles depended on the sugars and degrees of polymerization. Glycopolymers from pegylated-mannoside-functionalized polynorbornene, with $\overline{DP_n}$ = 100, showed strong binding inhibition, with subnanomolar range inhibitory concentrations (IC_{50s}). Polymers surpassed the inhibitory potential of their monovalent analogs by four to five orders of magnitude thanks to a multivalent (synergistic) effect. Sugar-functionalized poly(norbornenyl azlactone)s are therefore promising tools to study multivalent carbohydrate-lectin interactions and for applications against lectin-promoted bacterial/viral binding to host cells.

INTRODUCTION

Glycopolymers are carbohydrate-containing macromolecules made of a synthetic backbone with pendant sugars that are able to mimic naturally-derived polysaccharides.[1–6] These multivalent carbohydrates exhibit stronger molecular recognition of complementary carbohydrate-binding proteins (lectins) than individual monosaccharides in a number of important biological processes.[7] This "cluster-glycoside" effect can be attributed to an increased local concentration of active principle on protein glycan receptors.[8]

To date, glycopolymers have been mainly prepared by polymerization of carbohydrate-bearing monomers that must be synthesized beforehand.[9–13] The alternative approach involves click post-polymerization modification (PPM) of an existing polymer scaffold with sugar-bearing reagents. The scaffold acts as a platform offering rapid access to glycopolymer libraries with a broad scope of carbohydrate structures without tedious protection-deprotection sequences. Among the controlled/living polymerization techniques used,[14] ring-opening polymerization metathesis (ROMP) has been reported to produce well-defined products with high molar masses and high yields. In addition, the presence of carbon-carbon double bonds and cyclopentane along the polymer scaffold increases the rigidity of the structure, avoiding conformational entropy penalty and promoting target specificity.[4,5] The direct grafting of amino-terminated carbohydrates on a ROMP-based scaffold through click PPM by *N*-hydroxysuccinimide (NHS) functionality was reported by L. L. Kiessling.[15,16] Multivalent mannoses were obtained by PPM of a series of NHS-functionalized polynorbornene (PNB) scaffolds of number-average degrees of polymerization ($\overline{DP_n}$) ranging from 10 to 50 with an α-mannose derivative. The mannose-bearing PNB with a $\overline{DP_n}$ = 50 exhibited the highest inhibitory potencies against the lectin Concanavalin A (Con A).[16] Nevertheless, the NHS-activated ester group shows limitations, resulting in high background hydrolysis rates under the conditions of the conjugation reaction.[17,18] In addition, removing

the by-product (succinimide) can be challenging. The azlactone moiety has been shown to be a suitable click group to react with amino-terminated functional moieties with a high reactivity, a full atom economy in a broad range of organic solvents as well as in aqueous solution at room temperature.[19–21] Moreover, we previously demonstrated that the azlactone functionality is compatible with ruthenium-based catalysts[22,23], unlike the azido group.[24,25] Indeed, our group reported the synthesis of well-defined poly(norbornenyl azlactone) (**PNBAzl**) of $\overline{DP_n}$ = 50 to 225 from the *endo*/*exo* mixture of norbornenyl azlactone (**NBAzl**) using a third generation ruthenium-based catalyst (**G3′**).[26] In addition, aminolysis of the azlactone ring generates a bis-amide bond in a one-step post PPM[22,27] enabling the fast design of glycopolymers.[28] Carbohydrate ligands are therefore directly connected to the scaffold, preserving the rigidity of the structure for a perfect match with lectin proteins.

Given the lower reactivity of *endo*-substituted norbornenes[22, 29–31], in the present study we investigated the ROMP of each of the two diastereoisomers of **NBAzl**, namely ***endo*-** and ***exo*-NBAzl.** We used the pyridine-modified ruthenium-based **G3′** catalyst in order to obtain a library of scaffolds with a wide range of $\overline{DP_n}$. The subsequent PPM with amine-functionalized mannoside and glucoside ligands produced glycopolymers of different lengths. Mannose analogs were functionalized with a hydrophilic triethyleneglycol (TEG) spacer or hydrophobic heptyl chain. The latter was previously shown to enhance binding affinity for specific lectins (e.g., FimH from *E. coli* or DC-SIGN).[32,33] Finally, a TEG glucosyl was also prepared as a mismatch sugar for lectin assays. The binding inhibition of the resulting glucose- and mannose-functionalized **PNBAzl** with scaffolds of different lengths were evaluated against a set of model and therapeutically relevant lectins, using a "lectin profiling" technology. We selected five mannose-binding lectins (ConA, FimH, Bc2L-A, DC-SIGN, and langerin) for their biological relevance and marked sensitivity to multivalency. Concanavalin A (ConA) has long been studied as a model lectin for multivalency, due to its commercial

availability and its tetrameric structure with one carbohydrate binding site per subunit. Depending on the ligand architecture, ConA may precipitate with multivalent carbohydrates and glycoproteins or form well-ordered cross-linked lattices.[34] FimH and Bc2L-A are bacterial virulent factors used by *Escherichia coli* and *Burkholderia cenocepacia*, respectively, to adhere to host tissues by an oligosaccharide-mediated recognition. The design of Bc2L-A and FimH antagonists has been investigated as a way to develop antiadhesive compounds[35–37] as an alternative to antibiotics. Promising results have been obtained for the management of chronic and recurrent urinary tract infections promoted by *E. coli*.[38,39] Similarly, FimH antagonists were shown to decrease the level of adherent-invasive *E. coli* in the bowels of mice, which subsequently decreased the associated inflammatory syndromes, opening new avenues for the treatment of inflammatory bowel diseases.[40,41] DC-SIGN is a pathogen recognition receptor expressed at the surface of dendritic cells. It has an essential role in immune regulation but is hijacked by numerous bacteria, virus and fungi pathogens (such as HIV, Ebola virus, *C. albicans*) during their infection process. Much attention has been focused on the development of DC-SIGN antagonists.[42,43] For such an approach, the design of selective compounds is essential, as langerin, a related mannose-specific C-type lectin at the surface of Langerhans cells, was shown to contribute to virus elimination. Much effort has been devoted to finding glycomimetics with high affinity for these lectins. The present work underlines the high potential of size-optimized and sugar-functionalized **PNBAzl** for lectin binding.

EXPERIMENTAL SECTION

Materials. Information regarding materials is described in the Supporting Information.

Analytical Methods. Attenuated Total Reflectance (ATR) Fourier Transform Infra-Red (FT-IR) spectra were obtained using a Nicolet avatar 370 DTGS system or a Bruker Tensor 27 mountain equipped with the Specac® ATR diamond accessory. Spectra were obtained at regular time intervals in the MIR region of 4000-500 cm^{-1} with a resolution of 4 cm^{-1} (64 scans) and analyzed using OPUS software. High resolution mass spectra (HR-MS) were recorded on a Waters Xevo GL-XS Qtof spectrometer coupled to an Acquity H-class LC apparatus. The ionization sources were performed with the available methods (ESI+, ESI-, ASAP+, ASAP-). A tolerance of 5 ppm was applied between calculated and experimental values. Flash chromatography was performed on silica gel (40-63 μm from Macherey-Nagel) using Reveleris X² Grace apparatus. ^{1}H and ^{13}C NMR spectra were recorded on a Bruker Avance 400 or a Bruker Avance 300 spectrometer. Chemical shifts (δ) are expressed in ppm units, relative to the residual solvent peak. NMR spectra were assigned on the basis of the following 1D and 2D experiments: ^{1}H, ^{13}C, DEPT-135, COSY, HSCQ, HMBC. Coupling constants (*J)* are reported in Hz and peak multiplicities are noted according to the following abbreviations: s = singlet, d = doublet, t = triplet, q = quartet, quin = quintet, m = multiplet, dd = doublet of doublet, dt = doublet of triplet, br = broad signal. The molar masses (number-average molar mass $\overline{M_n}$, weight-average molar mass $\overline{M_w}$) and dispersity ($Đ = \overline{M_w}/\overline{M_n}$) values of the poly(norbornenyl azlactone)s were measured by Size Exclusion Chromatography (SEC) using tetrahydrofuran (THF) as an eluent, and carried out using a system equipped with a Waters 2707 autosampler, with a guard column (Waters, Styragel, 20 μm Guard column, 30 x 4.6 mm) followed by two columns (Waters, 2 Styragel THF HR2+HR4, 300 x 7.8 mm) and with a Waters RI-2414 detector. The instrument operated at a flow rate of 1.0 $mL.min^{-1}$ at 35°C and was calibrated with narrow linear polystyrene (PS) standards ranging in molar mass

from 580 g mol^{-1} to 483 000 g mol^{-1}. The molar masses (number-average molar mass $\overline{M_n}$, weight-average molar mass $\overline{M_w}$) and dispersity ($Đ = \overline{M_w}/\overline{M_n}$) values of the glycopolymers were measured by SEC using dimethyl sulfoxide (DMSO) with LiBr (1g/L)as an eluent, and carried out using a system equipped with an isocratic HPLC pump Waters 1515, a Waters 2707 plus autosampler, with a guard column (PSS gram, 10 µm Guard column, 8 x 50 mm) followed by two columns (PSS gram, linear 10 µm, 8 x 300 mm), all three stored in an oven at 70°C, with a photodiode array Waters 2998 detector and a differential Waters 2414 refractometer at 45°C. The instrument operated at a flow rate of 1.0 mL.min^{-1} at 35°C and was calibrated with narrow linear poly(methyl methacrylate) (PMMA) standards ranging in molar mass from 904 g mol^{-1} to 533 000 g mol^{-1}. Microwave-assisted syntheses were performed on a CEM Discover SP multimode cavity instrument using the Synergy software. All reactions were carried out with continuous stirring in a 10 mL sealed glass tube reactor containing 5−7 mL of the respective starting solution. The reaction temperature was maintained at 150°C by an external infrared surface sensor by using the power varying mode and reaction times were regarded as hold times at the setting temperature, not to total irradiation times.

Synthesis procedures. Details about the synthesis and the characterization of the *endo*- and *exo*-norbornenylazlactone, the three amino-functionalized carbohydrates: pegylated mannoside (**1a**, Scheme 3), heptyl-mannoside (**1b**, Scheme 3), and pegylated glucoside (**1c**, Scheme 3) and their acetyl analogs (**2a-c**, Scheme 3) are described in the Supporting Information.

General procedure for ROMP. In a typical experiment, a dry Schlenk tube was charged with the desired quantity of NBAzl and a stir bar. The Schlenk tube was capped with a rubber septum and subjected to five freeze–pump-thaw cycles. The desired amount of degassed, anhydrous DCE was added via a syringe under a nitrogen atmosphere to dissolve NBAzl

([NBAzl] = 0.487 mol.L^{-1}). A solution of G3′ in 0.2 mL of degassed anhydrous DCE was prepared in a separate vial. The Schlenk tube was then immersed in an oil bath preset to the desired temperature (Table 2) and the G3′ initiator solution was injected quickly into the monomer solution to initiate the polymerization (initial reaction time, t = 0). The Schlenk tube was stirred under argon for a reaction time ranging from 45 min to 36h (Table 2). Polymerizations were quenched by adding 0.2 mL of ethyl vinyl ether followed by 0.1 equiv. of potassium isocyanate used as a ruthenium scavenger. The resulting highly viscous green solution was then diluted in DCE and passed through a neutral alumina column. The resulting polymer was dried overnight under reduced pressure.

Kinetic studies. $[NBAzl]_0/[G3']_0 = 100$. A typical ROMP procedure was carried out. Aliquots of reaction mixture were taken at different reaction times and polymerization was quenched by adding two drops of ethyl vinyl ether for ^{1}H NMR spectroscopy analysis. Aliquots were passed through a neutral alumina column. The solvent of aliquots was then removed under reduced pressure for further SEC measurements to determine number-average molar masses ($M_{n,SEC}$) and dispersity ($Đ$).

General procedure for PPM of PNBAzl with amino-sugars. In a round bottom flask, P(*exo*-NBAzl) (10 mg) and amino-functionalized **1a-c** (1.2 equiv./Azl group) were dissolved in DMSO (1 mL) under argon. The resulting mixture was allowed to stir for 24 h at 50 °C. After cooling at room temperature, the mixture was transferred into dialysis tube MWCO 1 kDa (Spectra/por® 7), the reactor was rinced with DMSO (1 – 2 mL) and nanopore water (6 - 10 mL). Then dialysis was proceeded in 3 different baths against nanopure water (5 L) for 1h, 3h and 24h. The solution was finally freeze-dried to afford the desired functionalized polymer.

Lectin Array assays. They were performed according GlycoDiag's protocol already described[44–46]. Briefly, GLYcoPROFILEs were performed on LEctPROFILE® plates from GLYcoDiag (Orléans, France). The interaction profiles of each compound were determined

through an indirect method based on the inhibition by the compound of the interaction between a specific couple lectin-glycan (neoglycoprotein αMan-BSA: NeoM). Briefly, a mix of neoglycoprotein (fixed concentration) and the corresponding compounds (range of concentrations) prepared in PBS supplemented with 1 mM $CaCl_2$ and 0.5 mM $MgCl_2$ is deposed in each well (50 µL each) in triplicates and incubated two hours at room temperature. After washing with PBS buffer, the conjugate streptavidine-DTAF is added (50 µL) and incubated 30 min more. The plate was washed again with PBS. Finally, 100 µL of PBS was added for the readout of fluorescent plate performed with a fluorescence reader (λ_{ex} = 485 nm, λ_{em} = 530 nm, Fluostar OPTIMA, BMG LABTECH, France). The signal intensity is inversely correlated with the capacity of the compound to be recognized by the lectin and expressed as inhibition percentage with comparison with the corresponding tracer alone (neoglycoprotein).

RESULTS AND DISCUSSION

Synthesis of norbornenyl azlactone under microwave irradiation. Norbornenyl azlactone (**NBAzl**) is usually obtained by a two-step procedure via a Diels-Alder (DA) reaction between 2-vinyl-4,4-dimethyl-5-oxazolone (VDM) and cyclopentene (CPD) from freshly cracked dicyclopentadiene (DCPD) under thermal activation.[22] Herein, we developed a straightforward one-step procedure from VDM and DCPD, using microwave irradiation promoting both the *in situ* generation of CPD[47] and the DA reaction (Scheme 1).

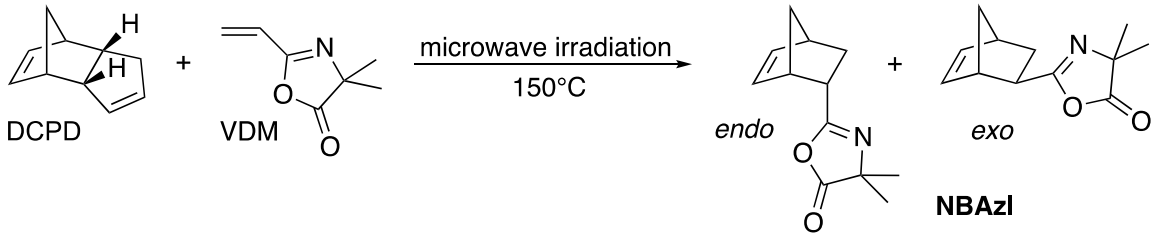

Scheme 1. Synthesis of **NBAzl** under microwave irradiation.

Reactions between VDM and DCPD under microwave conditions were first performed using different [CPD]/[VDM] ratios at 150°C (Table 1). When the DA reaction was performed with a [CPD]/[VDM] ratio of 1.1 and a reaction time of 1.5 h, a limited conversion of 33% was observed (entry 1, Table 1). Performing the reaction at a [CPD]/[VDM] ratio of 2.2 resulted in quantitative conversion (entry 2, Table 1). This procedure was then successfully applied from crude VDM to avoid tedious distillation issues that would otherwise result in product losses (entry 3, Table 1). Further experiments indicated that these reactions could be completed in 1 h with a [CPD]/[VDM] ratio of 2.6 instead of 2.2 (entries 5 vs. 4, Table 1). The *endo*/*exo* ratio of the **NBAzl** diastereoisomers was estimated to be 46/54 (Table 1). It is worth mentioning the excellent reproducibility of the *endo*/*exo* ratio resulting from this new synthesis protocol. Indeed, the values previously reported in the literature for **NBAzl**

synthesized by thermal activation showed a favored *endo* diastereoselectivity ranging from 60 to 75%[22,26], which can be explained by lack of uniformity of the oil bath temperature.

The *endo*/*exo* mixtures of **NBAzl** were separated by preparative high-performance liquid chromatography (HPLC) to isolate each of the pure ***exo*-NBAzl** and pure ***endo*-NBAzl** diastereoisomers.

Table 1. Experimental conditions, conversion, *endo*/*exo* ratio and yield for the Diels-Alder reactions between VDM and DCPD under microwave irradiation at 150°C.[a]

Entry	[CPD]/[VDM]	VDM	Reaction time (h)	Conv.[b] (%)	*endo*:*exo* ratio[c]	Yield (%)
1	1.1	distilled	1.5	33	47:53	-
2	2.2	distilled	1.5	> 99	46:54	69
3	2.2	crude	1.5	> 99	47:53	65
4	2.2	crude	1	87	47:53	-
5	2.6	crude	1	> 99	46:54	70

[a] Results are representative of at least duplicate experiments. [b] The conversion was determined by ^{1}H NMR based on comparison of the integrations of the VDM alkene proton signals at δ = 6.25–6.32 ppm (labeled orange, Figure S5A) with the ***exo*-NBAzl** cyclic alkene proton signals at δ = 6.15–6.22 ppm (labeled green, Figure S5A) and the ***endo*-NBAzl** cyclic alkene proton signals at δ = 5.80–5.90 ppm (labeled blue, Figure S5A) from ^{1}H NMR spectra of the crude mixtures. [c] The *endo*:*exo* ratio was determined by comparing the integrations of the signals related to the cyclic alkene protons in *endo*-position at δ = 5.80–5.90 and 6.23–6.29 ppm (labeled blue, Figure S5B in SI) and in *exo*-position at δ = 6.15–6.22 ppm (labeled green, Figure S5B in SI) from ^{1}H NMR spectra of the crude mixtures.

ROMP of *endo*- and *exo*-NBAzl. We first investigated the ROMP of ***endo*-** and ***exo*-NBAzl** using 1 mol% of Grubbs' third-generation catalyst (**G3′**, Figure S6A) in dichloroethane (DCE) at 70°C with a monomer-to-initiator molar ratio ($[NBAzl]_0/[\mathbf{G3'}]_0$) of 100 under the same conditions reported in a previous study for the ROMP of the *endo*/*exo* mixture of **NBAzl** (Scheme 2).[26] The ring-opening of the norbornene adduct was monitored by ^{1}H NMR analysis of the reaction mixture after termination by the addition of a small amount of ethyl

vinyl ether. Two broad resonance peaks appeared in the spectra at δ = 5.10–5.50 ppm (labeled b & c, Figure S7 in SI) and the cyclic alkene resonance disappeared at δ = 5.80–5.90 ppm (labeled $H_{2\text{-}3}$, Figure S3 in SI) and 6.15–6.22 ppm (labeled $H_{2\text{-}3}$, Figure S1 in SI) for ***endo***- and ***exo*-NBAzl**, respectively.

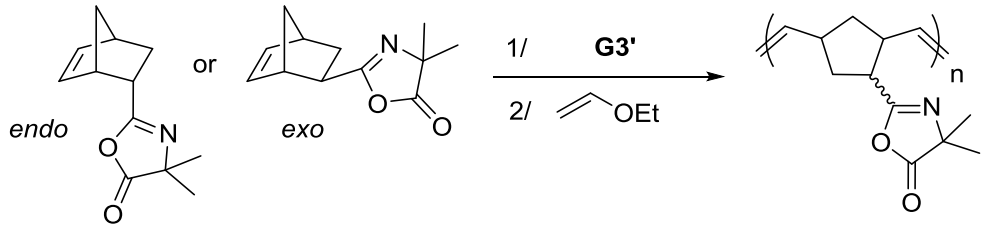

Scheme 2. ROMP of **NBAzl** using ruthenium-based initiator **G3'**.

While the ROMP of ***endo*-NBAzl** was completed in 36 h, ***exo*-NBAzl** polymerized faster, with a complete conversion after only 1 h of reaction (entry 1 *vs.* entry 4, Table 2). Decreasing the polymerization temperature to 25°C completely suppressed the ROMP of ***endo*-NBAzl** (entry 2, Table 2) whereas ***exo*-NBAzl** polymerized quantitatively in 36 h (entry 11, Table 2). In contrast, ***exo*-NBAzl** underwent complete polymerization at 50°C, with monomer-to-initiator molar ratios ranging from 10 to 1,000 (entries 5–10, Table 2) for a reaction time of 1.5 h. In addition, the conversion of ***exo*-NBAzl** with a monomer-to-initiator molar ratio of 1,000 for a reaction time of 36 h was quantitative at 25°C, whereas ROMP of ***endo*-NBAzl** showed a limited conversion of 32% for the same reaction time at a temperature of 70°C (entry 3 vs. entry 12, Table 2). The lower reactivity of ***endo*-NBAzl** towards ROMP is attributed either to steric reasons or to the chelating propensity of *endo*-substituted monomers[22,26,29–31,48–50] with the six-membered chelation of nitrogen to the ruthenium center (Figure S9 in SI). Steric exclusion chromatography (SEC) of the polymers after purification by passing the crude material through an alumina column showed unimodal profiles with a narrow dispersity (*Đ*) ranging from 1.12 to 1.38 (Figure S10 in SI). Furthermore, a linear

relationship was seen between the number-average molar masses ($M_{n,SEC}$) and the $[NBAzl]_0/[\mathbf{G3'}]_0$ ratio (Figure S11 in SI), indicating that the homopolymerization of ***exo*-NBAzl** is a well-controlled chain-growth polymerization.

Table 2. Characteristics of polymers obtained by ROMP of ***exo*** and ***endo*-NBAzl** using **G3′** initiator in DCE with varying monomer-to-initiator molar ratios.[a]

Entry	Monomer	$\frac{[NBAzl]_0}{[\mathbf{G3'}]_0}$	Temperature (°C)	Reaction time (h)	Conv.[b] %	$\overline{DP_{n,calc}}$[c]	$\overline{M_{n,calc}}$[d] g.mol^{-1}	$\overline{M_{n,SEC}}$[e] g.mol^{-1}	$Đ$[e]
1	***endo*-NBAzl**	100	70	36	> 99	99	20,400	20,500	1.14
2	***endo*-NBAzl**	100	25	36	0	0	0	-	-
3	***endo*-NBAzl**	1,000	70	36	32	320	65,900	79,300	1.39
4	***exo*-NBAzl**	100	70	1	100	100	20,600	28,100	1.14
5	***exo*-NBAzl**	10	50	1.5	100	10	2,600	2,400	1.35
6	***exo*-NBAzl**	50	50	1.5	100	50	10,350	13,100	1.14
7	***exo*-NBAzl**	100	50	1.5	100	100	20,600	27,200	1.12
8	***exo*-NBAzl**	250	50	1.5	100	250	51,400	61,900	1.15
9	***exo*-NBAzl**	500	50	1.5	100	500	102,600	149,700	1.17
10	***exo*-NBAzl**	1,000	50	24	100	1,000	206,000	290,000	1.38
11	***exo*-NBAzl**	100	25	36	> 99	99	20,400	21,000	1.13
12	***exo*-NBAzl**	1,000	25	36	> 99	990	203,000	246,700	1.28

[a] Results are representative of at least duplicate experiments [b] The monomer conversions were determined by comparing the integrations of alkene protons of the norbornene at δ = 5.80–6.22 ppm and the alkene protons of polymers at δ = 5.10–5.60 ppm from ^{1}H NMR spectra of the crude mixtures. [c] $\overline{DP_{n,calc}} = Conv. \times ([NBAzl]_0/[G3']_0)$. [d] $M_{n,calc} = \overline{DP_{n,calc}} \times M_{NBAzl} + M_{extr.}$ with M_{NBAzl} = 205 g.mol^{-1} and $M_{extr.}$ = 104 g.mol^{-1}. [e] Determined by SEC in tetrahydrofuran (THF) using an RI detector, calibrated with linear polystyrene (PS) standards.

The *cis*/*trans* ratio of the poly(norbornenyl azlactone)s (**PNBAzl**) was determined by quantitative ^{13}C NMR.[51] The assignment of *cis* and *trans* signals of the double bonds was performed by comparison with the ^{13}C NMR spectrum of a ***cis*-PNBAzl** obtained by ROMP of ***exo*-NBAzl** using 1 mol% of a *cis* selective Grubbs catalyst (Figure S6B in SI) in DCE at 50°C with a monomer-to-initiator molar ratio ($[NBAzl]_0/[\mathbf{G3'}]_0$) of 100 in 1.5 h (Figure S8B

in SI).[52] Comparison of the relative intensities of the methine carbons in α of the *cis* double bond at δ = 35.4–37.6 and 40.5–43.2 ppm (labeled a_{cis} and d_{cis}, Figures S8A and S8B in SI) and of the *trans* double bond at δ = 40.5–43.2 and 46.5–48.0 ppm (labeled a_{trans} and d_{trans}, Figure S8A in SI) indicated a predominant *cis* stereoregularity with a *cis*:*trans* ratio of 70:30 for both poly(*endo*-norbornenyl azlactone) (**P(*endo*-NBAzl)**) and poly(*exo*-norbornenyl azlactone) (**P(*exo*-NBAzl)**).

A sequential monomer addition experiment was carried out at 70°C in DCE. ROMP reactions of ***exo*-NBAzl** and ***endo*-NBAzl** involving a monomer-to-initiator molar ratio of 50 led to full conversions after 45 min and 36 h, respectively. In both cases, a new feed of monomer was added to the reaction mixture with a monomer-to-initiator molar ratio of 100 and the reaction was quenched with ethyl vinyl ether after 1 h for ***exo*-NBAzl** and 36 h for ***endo*-NBAzl**. The SEC profile shifted to a lower elution volume, while maintaining narrow dispersity values after monomer addition (Figure 1). About 5% of dead polymer chains were observed in **P(*endo*-NBAzl)**, as estimated from the SEC peak areas of the polymer before and after extension (Figure 1B). In contrast, the propagating chain-end of **P(*exo*-NBAzl)** was stable after ROMP for 60 min at 70°C (Figure 1A), showing its living character.

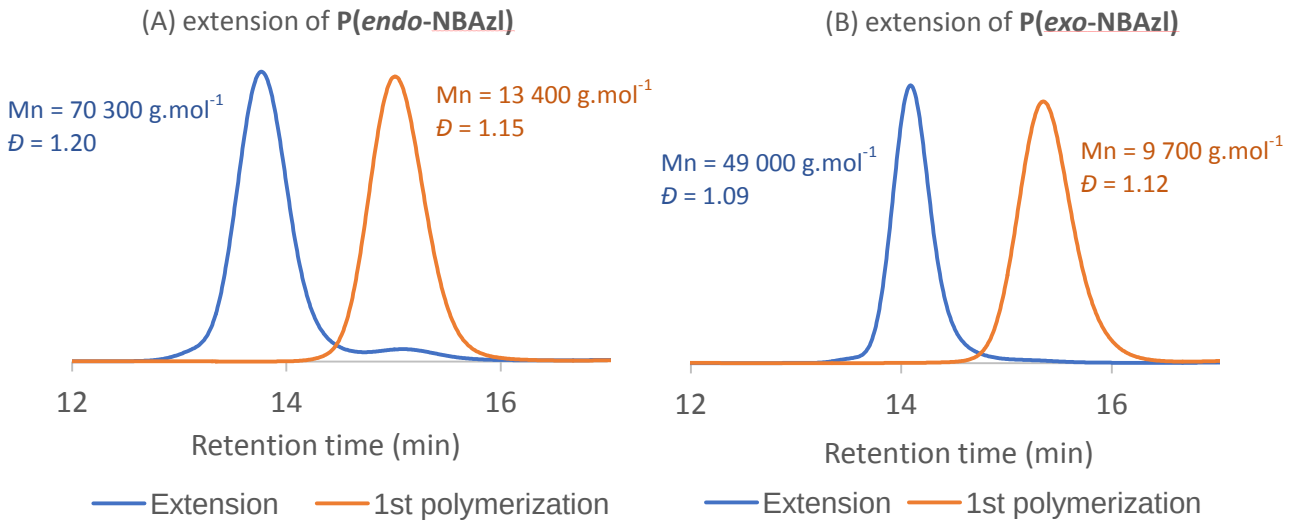

Figure 1. SEC profiles before and after monomer addition by chain extension ROMP of (A) **P(*endo*-NBAzl)** and (B) **P(*exo*-NBAzl)**.

Kinetic study of ROMP of *endo*- and *exo*-NBAzl. ROMP of ***endo*-** and ***exo*-NBAzl** with an initial monomer concentration of 0.05 mol.L^{-1} and a $[NBAzl]_0/[\mathbf{G3'}]_0$ ratio of 100 at 70°C in DCE were monitored by ^{1}H NMR spectroscopy. The linearity of the plots indicated linear pseudo-first-order behavior (Figures 2A & 2B). SEC chromatograms of crude polymers at different reaction times during ROMP of ***exo*-NBAzl** and ***endo*-NBAzl** (Fig. 2C & 2D) are symmetrical and shift to lower elution volumes with increasing polymerization time. The linear evolution of experimental molar masses as a function of conversion occurred for both polymerizations with narrow dispersity values, as shown in Figures 2E & 2F. To our great satisfaction, all these criteria taken together provide evidence of a well-controlled polymerization.

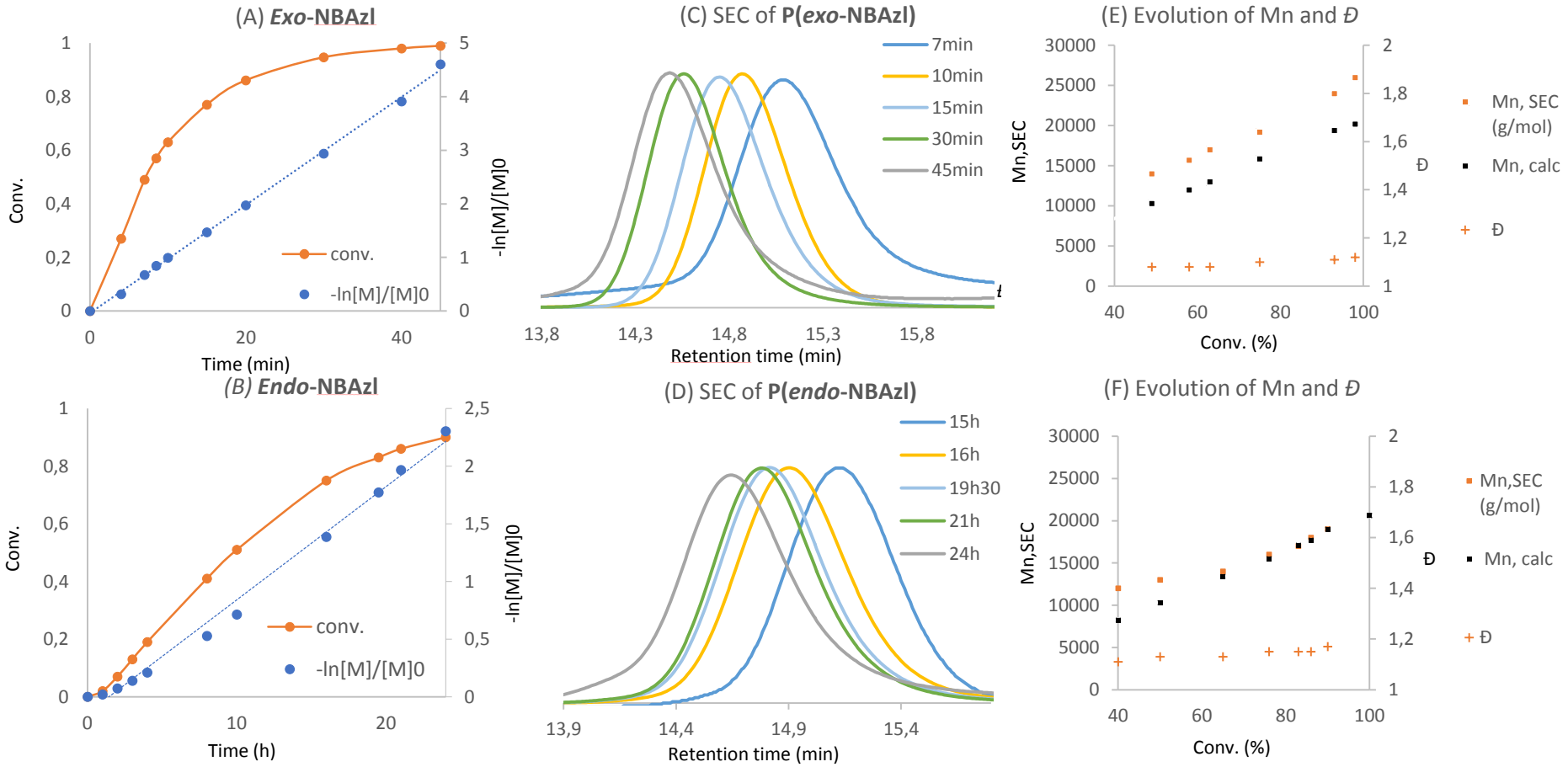

Figure 2. Kinetic plots – $\ln([M]_t/[M]_0)$ vs. reaction time for ROMP with an initial monomer concentration of 0.05 mol.L^{-1} and a $[NBAzl]_0/[$**G3'**$]_0$ ratio of 100 at 70°C in DCE of (A) ***exo*-NBAzl** and (B) ***endo*-NBAzl**. SEC traces of (C) crude **P(*exo*-NBAzl)** and (D) **P(*endo*-NBAzl)** at different conversions. $M_{n,SEC}$ and $Đ$ *vs.* conversion plots for (E) **P(*exo*-NBAzl)** and (F) **P(*endo*-NBAzl)**.

The values of the apparent propagation rate constants (k_p^{app}) determined from the slopes of the semi-logarithmic kinetic plots are given in Table 3. The k_p^{app} value obtained from ROMP of ***exo*-NBAzl** was understandably higher than that from ROMP of ***endo*-NBAzl** by a factor of 60. This result confirms the slower ROMP rate of ***endo*-NBAzl** as previously observed. It is worth mentioning the k_p^{app} = 0.0016 min^{-1} from ROMP of ***endo*-NBAzl** comparable to that from ROMP of an ***endo*/*exo*-NBAzl** mixture in a 67:33 ratio (k_p^{app} = 0.0015 min^{-1})[26], suggesting that ***endo*-NBAzl** has an inhibitory effect on the ROMP of ***exo*-NBAzl** and drives the kinetics of the ***endo*/*exo*-NBAzl** mixture.

Table 3. Kinetic data for ROMP of ***endo*-** and ***exo*-NBAzl** using **G3'** as the initiator with an initial monomer concentration of 0.05 $mol.L^{-1}$ and a $[NBAzl]_0/[\mathbf{G3'}]_0$ ratio of 100 at 70°C in DCE.

Entry[a]	monomer	Conv%[b]	Reaction time (h)	k_p^{app} [c]	k_p [d]
1	***exo*-NBAzl**	100%	0.75	0.0995	0.3316
2	***endo*-NBAzl**	90%	24	0.0016	0.0054
3	**NBAzl**[e]	90%	24	0.0015	0.0050

[a] Results are representative of at least duplicate experiments. [b] The conversion was determined by ^1H NMR, by comparing the integrations of the norbornene alkene protons at δ = 5.90–6.22 ppm and the alkene protons of polymers at δ = 5.10–5.60 ppm. [c] min^{-1}, calculated from the slopes of semilogarithmic kinetic plots. [d] $s^{-1}.L.mol^{-1}$. [e] *endo*/*exo*-NBAzl mixture at a 67:33 molar ratio.

Ring-opening metathesis polymerization of an ***endo*/*exo*-NBAzl** mixture in a 50:50 molar ratio at 25°C (temperature at which the ***endo*-NBAzl** alone does not polymerize at all) was performed with an initial monomer concentration of 0.05 $mol.L^{-1}$ and a $[NBAzl]_0/[\mathbf{G3'}]_0$ ratio of 100 in DCE. The conversion of each monomer was monitored by comparing the integrations of the alkene protons of the ***endo*-** and ***exo*-NBAzl** at δ = 5.90–6.22 ppm, respectively, and the alkene protons of the polymers at δ = 5.10–5.60 ppm. Results showed that ***endo*-NBAzl** polymerizes at 25°C in the presence of ***exo*-NBAzl** according to pseudo-

first order kinetics (Figure S12A in SI). The molar mass increased with the conversion while retaining a dispersity value < 1.3 as expected for a well-controlled ROMP (Figures S12B and S12C in SI). After 150 h of reaction, the overall monomer conversion reached 75% (Figure S12A in SI), with a higher conversion of the more reactive ***exo*-NBAzl** diastereoisomer than the ***endo*-NBAzl** (85% vs. 65%).

Post-polymerization modification with amino-functionalized carbohydrates. A one-step post-polymerization modification (PPM) of the **P(*exo*-NBAzl)** with $\overline{DP_n}$ ranging from 10 to 250 was performed with three amino-functionalized carbohydrates: pegylated mannoside (**TEG-Man**), heptyl-mannoside (**HMan**), and pegylated glucoside (**TEG-Glc**), creating a library of glycopolymers with different sugar identities and different lengths (Scheme 3). Depending on the length of the polymeric scaffold, different degrees of binding activity are expected.

Amino-functionalized glycosides **TEG-Man** (**1a**), **HMan** (**1b**), and **TEG-Glc** (**1c**) were prepared from acetylated glycosides by a four-step procedure consisting in glycosylation, azidation, deprotection, and hydrogenation.

The general route to the production of the glycopolymers relies on the ability of **P(*exo*-NBAzl)** to act as a versatile "clickable" polymeric scaffold able to efficiently react with primary amine-based nucleophiles.[53–55] Briefly, the click grafting of **P(*exo*-NBAzl)** with glycosides **TEG-Man**, **HMan**, and **TEG-Glc** was simply performed in dimethyl sulfoxide (DMSO) at 50°C with a 1.2:1 molar ratio of glycoside to azlactone-ring unit (Scheme 3B). After a dialysis step, good yields of all new glycopolymers were obtained, ranging from 55% to 99% after freeze drying (Table S1 in SI). Whatever the value of $\overline{DP_n}$ for a given family of glycopolymers, similar profiles in NMR and Fourier-Transform Infra-Red (FT-IR) analysis

were obtained. In the following, we therefore present the results of the PPM of the polymers with a $\overline{DP_n}$ = 50 (NMR: Figures S13–S18; FT-IR: Figure S19 in SI).

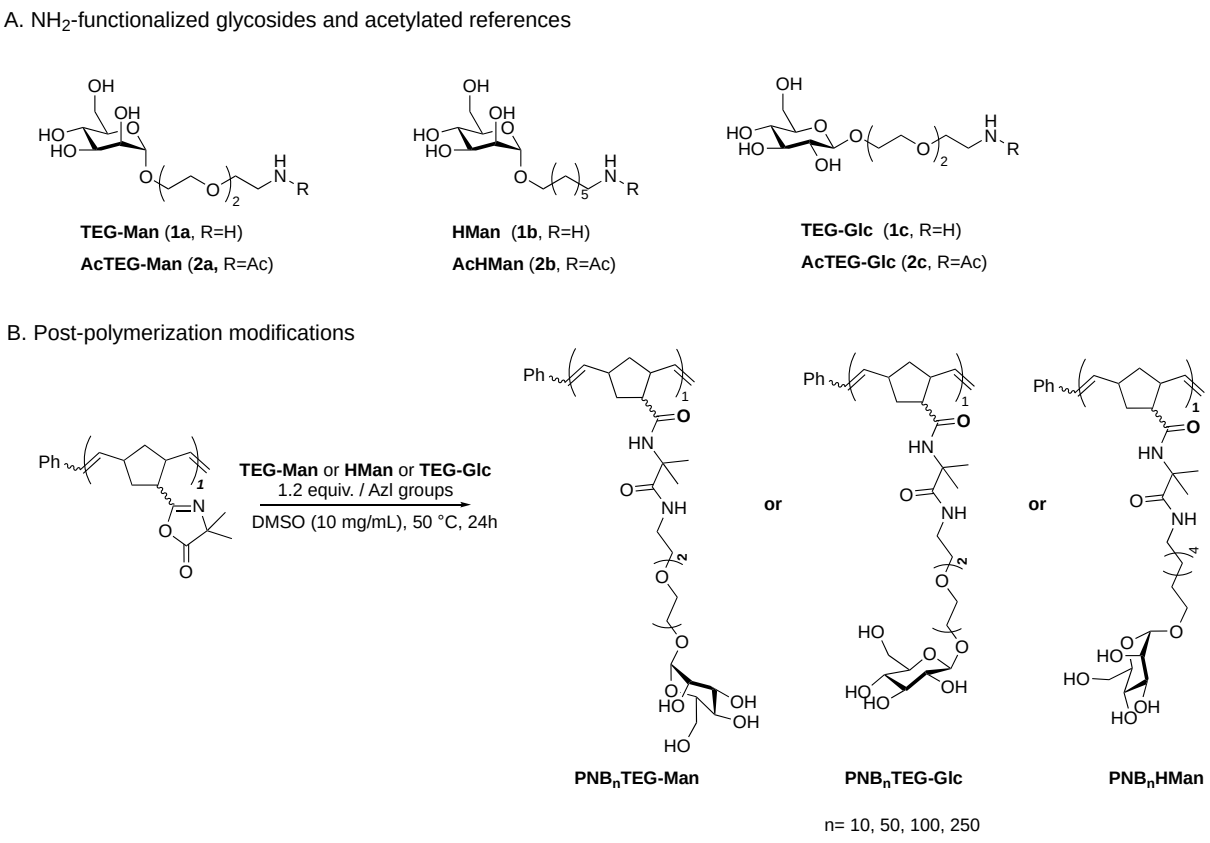

Scheme 3. PPM of **P(*exo*-NBAzl)**s with amino-functionalized sugars

For the three glycopolymers, the complete opening of azlactone ring was confirmed by FT-IR spectroscopy with the disappearance of the azlactone C=O (1813 cm^{-1}) and C=N (1668 cm^{-1}) stretching bands and the concomitant appearance of bands at (*i*) 3,310–3,320 cm^{-1} attributed to O-$H_{(sugar)}$ stretching and amide N-H symmetric stretching and (*ii*) 1,520–1,532 cm^{-1} attributed to N-H bending of secondary amides (Figures S19B, S19C and S19D vs. Figure S19A in SI).[26]

For **PNB_n-TEG-Man**, the incorporation of mannosides is evidenced by the signal of the anomeric proton at δ = 4.64 ppm ($J_{1,2}$ < 1.0 Hz, labeled k', Figure S13B in SI) and those of hydroxyl groups at δ = 4.67 ppm, 4.50 ppm, and 4.40 ppm. The emergence of signals in the

range δ = 3.00–3.68 ppm was attributed to the triethylene glycol chain. The bond between TEG and amide was characterized by a downfield chemical shift of the carbon in α of the amide from 39 to 51 ppm, respectively (labeled j', Figure S14 in SI).

For **PNB_n-HMAn**, the broad singlets of the vinyl protons of the backbone were found at δ = 5.19–5.32 ppm (Figure S15B in SI). At δ = 4.58 ppm, a singlet signal attributed to the anomeric proton was observed as well as the appearance of hydroxyl groups at δ = 4.64 ppm, 4.48 ppm, and 4.38 ppm. Alkyl chains were clearly highlighted in NMR ^{13}C spectra with typical chemical shifts at δ = 29.0–25.7 ppm (Figure S16).

For **PNB_n-TEG-Glc**, anomeric protons were characterized as a doublet at δ = 4.15 ppm (J = 7.7 Hz, labeled m', Figure S17B). New signals at δ = 7.31–7.53 ppm attributed to both the formed amide and deshielding of C_α of the amide ($C_{j'}$, Figure S18 in SI) provided evidence of the complete incorporation of glucosyl patterns.

The carbohydrate-functionalized polymers obtained after dialysis against water followed by a further lyophilization were analyzed by SEC in DMSO. All SEC traces show a shift to lower elution time after PPM of **P(*exo*-NBAzl),** which is consistent with the increase in molar mass and hydrodynamic volume resulting from the grafting reaction (Figures S20-S22 in SI). While the SEC traces of **PNB_n-TEG-Man** (Figures S20A to S20C in SI) and **PNB_n-TEG-Glc** (Figures S22A to S22C in SI) with a $\overline{DP_n}$ = 10 to 100 displayed a monomodal distribution with rather narrow dispersity values ranging from $Đ$ = 1.17 to 1.32, the SEC traces of **PNB_{250}-TEG-Man**, **PNB_{250}-TEG-Glc**, and all **PNB_n-HMan** exhibited very broad distributions, resulting in dispersity values ranging from 1.30 to 2.08 (Figures S20D, S21 and S22D in SI). The broadness of the peaks may be attributed to significant aggregation that occurs, as confirmed by dynamic light scattering (DLS) measurements (Figure S23 in SI).

Prior to lectin assays, monovalent glycoside references were prepared in order to compare the binding potency and synergistic effect of the multivalent glycoclusters. Designing full

glycoside-functionalized **NBAzl** monomers was envisaged to be structurally closer to polymers. Unfortunately, their poor solubility in water was detrimental to biological assays. We thus decided to use monovalent pegylated mannoside, heptyl-mannoside, and pegylated glucoside with an acetylated amine, respectively noted as **Ac-TEG-Man** (**2a**), **Ac-HMan** (**2b**), and **Ac-TEG-Glc** (**2c**) (Scheme 3A; complete synthetic pathways and characterizations are provided in SI).

Binding inhibition of the polymeric sugars. The binding inhibition of the whole set of polymeric sugars was evaluated against carbohydrate-binding proteins (lectins) using a "lectin profiling" technology (GLYcoPROFILE® from GLYcoDiag).[46] This method was shown to give reproductible IC50, even on complex glycol-nanosystems,[56] and similar inhibitory trends were observed by surface plasmon resonance (SPR).[57] The five lectins were coated on microplate surfaces and a labeled competitive ligand was designed, consisting of bovine serum albumin (BSA) decorated with mannosides (neoglycoprotein (NeoM)). The labeled BSA–lectin interaction on the biochip could be displaced with increasing concentrations of the competitive polymeric sugars. The proportional decrease of fluorescence intensity allowed determination of the half maximal inhibitory concentration of binding (IC_{50}) for each polymer. The relative inhibitory potency of a polymer compared with a monovalent reference is calculated as: RP = IC_{50}^{Mv}/ IC_{50}^{Pv}. To directly assess the level of a potential synergistic inhibitory effect, the RP value is divided by the number n of ligands attached to the polymer. A significant multivalent effect is achieved only if RP/n > 1.

The monovalent references showed relatively similar inhibition profiles for the five lectins, with weak inhibitory values in the high micromolar to low millimolar range (0.073–3.2 mM), as typically observed with monomeric sugars (Figure S24 in SI).[42] Except for Bc2L-A, the lectins showed a significant preference for the mannoside **Ac-TEG-Man** over the glucoside

Ac-TEG-Glc series, consistent with their previously known inhibition profiles. Although the affinity of Bc2L-A was previously documented for different monosaccharides,[58] we could not find indicative values for glucosides and the lectin may accommodate this sugar in its binding site as suggested by the inhibitory value of **Ac-TEG-Glc** (IC_{50} = 416 µM). Substitution of the TEG in **Ac-TEG-Man** by an heptyl chain in **Ac-HMan** led to IC_{50} values of the same order of magnitude except for DC-SIGN and FimH lectins, which showed a two-fold increase and decreased affinity for the respective lectins. This trend is in accordance with the reported preference of DC-SIGN for heptyl mannosides,[33] but we expected a significantly higher affinity for FimH, which can accommodate hydrophobic aglycons in its binding site.[59]

A preliminary assay performed on the polymers of $\overline{DP_n}$ ~ 10 and 50 showed improvements of the RP values compared with the sugar references in most cases (Figure S25 in SI). This effect was, however, highly dependent on the nature of the coated ligand. While moderate multivalent effects were observed with the set of **PNB-HMan** and **PNB-TEG-Glc** polymers bearing the heptyl spacer and the glucose ligand, respectively, strong synergistic effects were observed with **PNB-TEG-Man** (Table 4, Figure 3). The higher effect observed with **PNB-TEG-Man** polymeric mannosides over **PNB-TEG-Glc** glucosides reflects the known preference of the lectins for the mannose residue. We hypothesized that the disappointing inhibition observed with the **PNB-HMan** polymers with a heptyl tail could be explained by a higher hydrophobicity. Indeed, **PNB-HMan** were shown to form large aggregates in solution, as evidenced by SEC and DLS characterization (Figures S21 and S23 in SI), and were poorly water soluble during the biochip assay. These preliminary results led us to select the **PNB-TEG-Man** family with $\overline{DP_n}$ ~ 10 to 250 for a full evaluation in the biochip assay. Titration curves presented in Figure 3 showed rather similar inhibition profiles observed on the five lectins, with a very high inhibitory potencies achieved by the longest polymers ($\overline{DP_n}$ 100 and 250) on the whole panel of lectins.

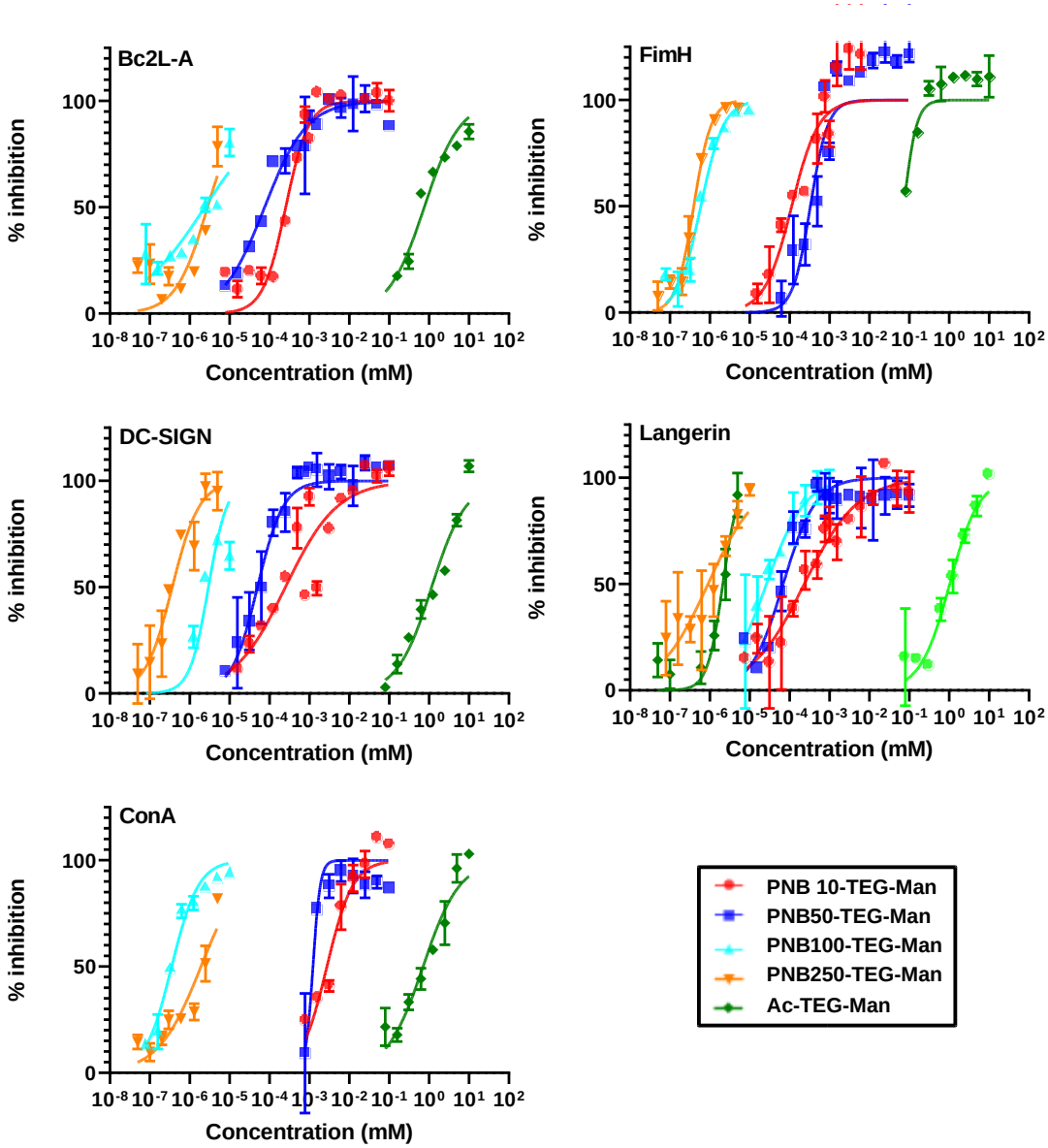

Figure 3. Titration curves of the monovalent reference **Ac-TEG-Man** and the corresponding **PNB$_n$-TEG-Man** mannose polymers obtained after a biochip assay. The lectins were immobilized on a plate and their interaction with a labeled and mannosylated BSA was measured. Then, competitive experiments were performed with **PNB$_n$-TEG-Man** compounds to determine IC_{50} values. Experiments were performed in triplicate.

IC_{50} values for **PNB-TEG-Man** (Table 4) are in the low nano- and subnanomolar range depending on the lectins, which represents an increase in binding potency by more than 5 to 6

orders of magnitudes (RP values) compared with the monovalent reference **Ac-TEG-Man**. The highest synergistic (multivalency) effect was observed with **PNB_{100}-TEG-Man**. The mannosides grafted on the polymer scaffold had 20,286 and 11,500-fold enhanced inhibitory efficiency (RP/n value) on ConA and langerin, respectively. compared with monovalent **Ac-TEG-Man**. High RP/n values were also observed on FimH (1,223-fold compared with **Ac-TEG-Man**), which is striking considering the different architectures of the monomeric FimH and the tetrameric ConA. While the enhanced activity on ConA may be explained by a binding mode where ligands from the polymers embrace several binding sites simultaneously, this chelate interaction is precluded with the monovalent FimH. Here, the synergy may be explained by a multivalent display of the lectin at the biochip surface, or by an internal diffusion mechanism where the mannosides are bound and recaptured by the lectin in a zip-like fashion, as previously described for GalNac binding lectins.[4] **PNB_{100}-TEG-Man** showed the highest RP/n values against Bc2L-A, FimH, langerin, and ConA, with further elongation of the polymer chain to $\overline{DP_n}$ 250 leading to a decreased multivalent effect. Such a threshold in multivalency is often observed when the ligand valency or density is increased.[60]

Altogether, results from the biochip assay showed that **PNB-TEG-Man** glycopolymers display inhibitory potencies and levels of multivalent effects rarely reported for carbohydrate-binding proteins. The polymer scaffolds presented here are therefore valuable tools to study multivalency and to design strong inhibitors of biologically relevant targets.

Table 4. Inhibitory activities of **PNB-TEG-Man** compounds measured by a biochip assay. Molecular inhibitory concentration values (IC_{50}) are given in micromolar units. The relative potency (RP) of a given polymer was calculated by dividing IC_{50} of the monovalent reference **Ac-TEG-Man** by the IC_{50} of the polymer. The valency-corrected relative inhibitory potencies (RP/n) show the enhancement factor of each clustered mannoside compared with **Ac-TEG-Man**.

		FimH		Bc2L-A		ConA	
Compounds	Valency	IC_{50} µM (RP)	RP/n	IC_{50} µM (RP)	RP/n	IC_{50} µM (RP)	RP/n
Ac-TEG-Man	1	$73 \pm 3.9.10^{2}$ (1)	1	$760 \pm 3.4.10^{3}$ (1)	1	$710 \pm 3.1.10^{3}$ (1)	1
PNB_{10}-TEG-Man	10	$0.11 \pm 1.0.10^{-1}$ (663)	66	$0.26 \pm 9.0.10^{-2}$ (2,923)	292	$2.8 \pm 1.2.10^{0}$ (254)	25
PNB_{50}-TEG-Man	50	$0.33 \pm 2.1.10^{-1}$ (221)	4.4	$0.076 \pm 2.0.10^{-2}$ (10,000)	200	$1.23 \pm 1.0.10^{0}$ (577)	12
PNB_{100}-TEG-Man	100	$0.000597 \pm 1.8.10^{-4}$ (122,278)	1223	$0.0024 \pm 2.9.10^{-3}$ (316,666)	3167	$0.00035 \pm 1.0.10^{-4}$ (2,028,571)	20286
PNB_{250}-TEG-Man	250	$0.000398 \pm 0.7.10^{-5}$ (183,417)	734	$0.0028 \pm 2.0.10^{-3}$ (271,429)	1086	$0.0019 \pm 1.5.10^{-3}$ (373,684)	1495
		DC-SIGN		Langerin			
Cpds	Valency	IC_{50} µM (RP)	RP/n	IC_{50} µM (RP)	RP/n		
Ac-TEG-Man	1	$1169 \pm 5.6.10^{3}$ (1)	1	$1035 \pm 3.0.10^{3}$ (1)	1		
PNB_{10}-TEG-Man	10	$0.25 \pm 1.8.10^{-1}$ (4,676)	468	$0.23 \pm 8.0.10^{-2}$ (4,500)	450		
PNB_{50}-TEG-Man	50	$0.050 \pm 1.2.10^{-2}$ (23,380)	468	$0.069 \pm 2.6.10^{-2}$ (15,000)	300		
PNB_{100}-TEG-Man	100	$0.0030 \pm 5.0.10^{-4}$ (389,667)	3897	$0.00090 \pm 6.0.10^{-4}$ (1,150,000)	11500		
PNB_{250}-TEG-Man	250	$0.00037 \pm 1.3.10^{-4}$ (3,159,459)	12638	$0.0021 \pm 6.2.10^{-4}$ (492,857)	1971		

CONCLUSIONS

In conclusion, new glycopolymers based on polynorbornenes bearing amino-functionalized glycosides in the side chain were developed. Norbornenyl azlactone was efficiently prepared through a straightforward procedure based on the Diels-Alder cycloaddition of 2-vinyl-4,4-dimethyl-5-oxazolone and dicyclopentadiene under microwave irradiation. Such a one-step protocol avoids the tedious purification procedures hitherto implemented for the preparation of this monomer. Each of the diastereoisomers, namely ***endo***- and ***exo*-NBAzl,** was isolated and subjected to ROMP using a pyridine-modified ruthenium-based third generation catalyst. Propagation rate constants determined through kinetic studies demonstrated a much higher reactivity of the *exo* diastereoisomer. While the *endo* diastereoisomer inhibits polymerization, preventing high molar masses from being achieved, poly(norbornenyl azlactone)s with an unprecedented range of $\overline{DP_n}$ (10 to 1,000) can be obtained using the *exo* diastereoisomer.

These azlactone-functionalized polynorbornenes served as a reactive platform for post-polymerization modification through click aminolysis using amino-functionalized glycosides. A library of glycopolymers of different lengths was thus easily obtained from **TEG-Man**, **HMan**, and **TEG-Glc**.

The biochip assay showed the high inhibitory potential of the **PNB-TEG-Man** glycopolymers against the whole panel of therapeutically relevant lectins (Bc2L-A, FimH, DC-SIGN and langerin). High synergistic effects were observed with **PNB_{100}-TEG-Man** of optimal size, that showed up to 20,000 fold (valency-corrected) enhanced inhibitory efficiency compared with the monovalent reference **Ac-TEG-Man**. Such levels of multivalent effects are rarely reported in literature, even for polymers.

Taken together, the results reported here demonstrate that poly(norbornenyl azlactone) is a valuable scaffold for designing multivalent systems strongly binding to biologically-relevant receptors.

ASSOCIATED CONTENT

Supporting Information

The Supporting Information is available free of charge.

Materials and synthetic procedures, ^{1}H NMR, ^{13}C NMR spectra, and FT-IR spectra, SEC chromatograms, and titration curves (pdf).

AUTHOR INFORMATION

Corresponding Authors

Laurent Fontaine – *Institut des Molécules et Matériaux du Mans (IMMM), UMR 6283 CNRS – Le Mans Université, Avenue Olivier Messiaen, 72085 Le Mans Cedex 9, France*; orcid.org/0000-0003-0043-1508; Email : laurent.fontaine@univ-lemans.fr

Véronique Montembault – *Institut des Molécules et Matériaux du Mans (IMMM), UMR 6283 CNRS – Le Mans Université, Avenue Olivier Messiaen, 72085 Le Mans Cedex 9, France*; orcid.org/0000-0003-3112-6768; Email : veronique.montembault@univ-lemans.fr

Authors

Clément Gonnot – *Institut des Molécules et Matériaux du Mans (IMMM), UMR 6283 CNRS – Le Mans Université, Avenue Olivier Messiaen, 72085 Le Mans Cedex 9, France*;

Mathieu Scalabrini – *Nantes Université, CNRS, CEISAM UMR 6230, F-44000 Nantes, France*

Benoit Roubinet – *GLYcoDiag, 2 rue du Cristal, 45100 Orléans, France*

Célia Ziane – *Institut des Molécules et Matériaux du Mans (IMMM), UMR 6283 CNRS – Le Mans Université, Avenue Olivier Messiaen, 72085 Le Mans Cedex 9, France*;

Fabien Boeda – *Institut des Molécules et Matériaux du Mans (IMMM), UMR 6283 CNRS – Le Mans Université, Avenue Olivier Messiaen, 72085 Le Mans Cedex 9, France*;

David Deniaud – *Nantes Université, CNRS, CEISAM UMR 6230, F-44000 Nantes, France*

Ludovic Landemarre – *GLYcoDiag, 2 rue du Cristal, 45100 Orléans, France*

Sébastien Gouin – *Nantes Université, CNRS, CEISAM UMR 6230, F-44000 Nantes, France;* orcid.org/0000-0002-0985-1165

Author Contributions

The manuscript was written through contributions of all authors.

Notes

The authors declare no competing financial interest.

ACKNOWLEDGEMENTS

This work was financed by Le Mans University, the Centre National de la Recherche Scientifique (CNRS), and the National Agency for Research (CyClick project, ANR-20-CE06-0025-01). Kexin Zhang, Alexandre Bénard and Sullivan Bricaud are acknowledged for their technical assistance in SEC analyses and NMR analyses, respectively.

REFERENCES

(1) Rawat, M.; Gama, C. I.; Matson, J. B.; Hsieh-Wilson, L. C. Neuroactive Chondroitin Sulfate Glycomimetics. *J. Am. Chem. Soc.* **2008**, *130*, 2959–2961.

(2) Ting, S. R. S.; Chen, G.; Stenzel, M. H. Synthesis of glycopolymers and their multivalent recognitions with lectins. *Polym. Chem.* **2010**, *1*, 1392–1412.

(3) Yilmaz, G.; Becer, C. R. Precision glycopolymers and their interactions with lectins. *Eur. Polym. J.* **2013**, *49*, 3046–3051.

(4) Dam, T. K.; Gerken, T. A.; Cavada, B. S.; Nascimento, K. S.; Moura, T. R.; Brewer, C. F. Binding Studies of α-GalNAc-specific Lectins to the α-GalNAc (Tn-antigen) Form of Porcine Submaxillary Mucin and Its Smaller Fragments. *J. Biol. Chem.* **2007**, *282*, 28256–28263.

(5) Wittmann, V.; Pieters, R. J. Bridging lectin binding sites by multivalent carbohydrates. *Chem. Soc. Rev.* **2013**, *42*, 4492–4503.

(6) Liese, S.; Netz, R.R. Quantitative Prediction of Multivalent Ligand− Receptor Binding Affinities for Influenza, Cholera, and Anthrax Inhibition. *ACS Nano* **2018**, *12*, 4140–4147.

(7) Yilmaz, G.; Becer, C. R. In *Carbohydrate Nanotechnology*, 1st ed.; Stine, K. J. Eds.; Wiley & Sons, Inc.: Hoboken, NJ, 2016; vol 16, pp. 137–174.

(8) Ladmiral, V.; Melia, E.; Haddleton, D. M. Synthetic glycopolymers: an overview. *Eur. Polym. J.* **2004**, *40*, 431–449.

(9) Gordon, E. J.; Gestwicki, J. E.; Strong, L. E.; Kiessling, L. L. Synthesis of end-labeled multivalent ligands for exploring cell-surface-receptor–ligand interactions. *Chem. Biol.* **2000**, *7*, 9–16.

(10) Huang, H.; Rodolis, M. T.; Bhatia, S. R.; Sampson, N. S. Sugars Require Rigid Multivalent Displays for Activation of Mouse Sperm Acrosomal Exocytosis. *Biochem.* **2017**, *56*, 2779–2786.

(11) Sletten, E. T.; Loka, R. S.; Yu, F.; Nguyen, H. M. Glycosidase Inhibition by Multivalent Presentation of Heparan Sulfate Saccharides on Bottlebrush Polymers. *Biomacromolecules* **2017**, *18*, 3387–3399.

(12) Fan, F.; Cai, C.; Wang, W.; Gao, L.; Li, J.; Li, J.; Gu, F.; Sun, T.; Li, J.; Li, C.; Yu, G. Synthesis of Fucoidan-Mimetic Glycopolymers with Well-Defined Sulfation Patterns via Emulsion Ring-Opening Metathesis Polymerization. *ACS Macro Lett.* **2018**, *7*, 330–335.

(13) Fan, F.; Cai, C.; Gao, L.; Li, J.; Zhang, P.; Li, G.; Li, C.; Yu, G. Microwave-assisted synthesis of glycopolymers by ring-opening metathesis polymerization (ROMP) in an emulsion system. *Polym. Chem.* **2017**, *8*, 6709–6719.

(14) Zhang, Q.; Haddleton, D. M. In *Advances in Polymer Science*; Percec, V. Eds.; Springer-Verlag Berlin Heidelberg, 2013; vol 262, pp. 39–60.

(15) Mann, D. A.; Kanai, M.; Dustin, J.; Kiessling, L. L. Probing Low Affinity and Multivalent Interactions with Surface Plasmon Resonance: Ligands for Concanavalin A. *J. Am. Chem. Soc.* **1998**, *1201*, 10575–10582.

(16) Strong, L. E.; Kiessling, L. L. A General Synthetic Route to Defined, Biologically Active Multivalent Arrays. *J. Am. Chem. Soc.* **1999**, *121*, 6193–6196.

(17) Wong, S. Y.; Putnam, D. Overcoming Limiting Side Reactions Associated with an NHS-Activated Precursor of Polymethacrylamide-Based Polymers. *Bioconjugate Chem.* **2007**, *18*, 970–982.

(18) Ho, H. T.; Bénard, A.; Forcher, G.; Le Bohec, M.; Montembault, V.; Pascual, S.; Fontaine, L. Azlactone-based heterobifunctional linkers with orthogonal clickable

groups: efficient tools for bioconjugation with complete atom economy. *Org. Biomol. Chem.* **2018**, *16*, 7124–7128.

(19) Laquièvre, A.; Allaway, N. S.; Lyskawa, J.; Woisel, P.; Lefebvre, J.-M.; Fournier, D. Highly Efficient Ring-Opening Reaction of Azlactone-Based Copolymer Platforms for the Design of Functionalized Materials. *Macromol. Rapid Commun.* **2012**, *33*, 848–855.

(20) Speetjens, F. W.; Carter, M. C. D.; Kim, M.; Gopalan, P.; Mahanthappa, M. K.; Lynn, D. M. Post-Fabrication Placement of Arbitrary Chemical Functionality on Microphase-Separated Thin Films of Amine-Reactive Block Copolymers. *ACS Macro Lett.* **2014**, *3*, 1178–1182.

(21) Quek, J. Y.; Liu, X.; Davis, T. P.; Roth, P. J.; Lowe, A. B. RAFT-prepared α-difunctional poly(2-vinyl-4,4-dimethylazlactone)s and their derivatives: synthesis and effect of end-groups on aqueous inverse temperature solubility. *Polym. Chem.* **2015**, *6*, 118–127.

(22) Lapinte, V.; Brosse, J.-C.; Fontaine, L. Synthesis and Ring-Opening Metathesis Polymerization (ROMP) of (±)-*endo*- and (±)-*exo*-Norbornenylazlactone using Ruthenium Catalysts. *Macromol. Chem. Phys.* **2004**, *205*, 824–833.

(23) Lapinte, V.; Fontaine, L.; Montembault, V.; Campistron, I.; Reyx, D. Ring-opening metathesis polymerization (ROMP) of isomerically pure functional monomers and acyclic diene metathesis depolymerization (retro-ADMET) of functionalized polyalkenamers. *J. Mol. Catal. A: Chem.* **2002**, *190*, 117–129.

(24) Xia, Y.; Verduzco, R.; Grubbs, R. H.; Kornfield, J. A. Well-Defined Liquid Crystal Gels from Telechelic Polymers. *J. Am. Chem. Soc.* **2008**, *130*, 1735-1740.

(25) Leitgeb, A.; Wappel, J.; Slugovc, C. The ROMP toolbox upgraded. *Polymer* **2010**, *51*, 2927–2946.

(26) François, F.; Nicolas, C.; Forcher, G.; Fontaine, L.; Montembault, V. Poly(norbornenyl azlactone) as a versatile platform for sequential double click postpolymerization modification. *Eur. Polym. J.* **2020**, *141*, 11008.

(27) Das, A.; Theato, P. Activated Ester Containing Polymers: Opportunities and Challenges for the Design of Functional Macromolecules. *Chem. Rev.*, **2016**, *116*, 1434–1495.

(28) Jones, M. W.; Richards, S.-J.; Haddleton, D. M.; Gibson, M. I. Poly(azlactone)s: versatile scaffolds for tandem post-polymerisation modification and glycopolymer synthesis. *Polym. Chem.* **2013**, *4*, 717–723.

(29) Rule, J. D.; Moore, J. S. ROMP Reactivity of *endo*- and *exo*-Dicyclopentadiene. *Macromolecules* **2002**, *35*, 7878–7882.

(30) Nishihara, Y.; Inoue, Y.; Nakayama, Y.; Shiono, T.; Takagi, K. Comparative Reactivity of Exo- and Endo-Isomers in the Ru-Initiated Ring-Opening Metathesis Polymerization of Doubly Functionalized Norbornenes with Both Cyano and Ester Groups. *Macromolecules* **2006**, *39*, 7458–7460.

(31) Moatsou, D.; Hansell, C.F.; O'Reilly, R.K. Precision polymers: a kinetic approach for functional poly(norbornenes). *Chem. Sci.* **2014**, *5*, 2246–2250.

(32) Bouckaert, J.; Berglund, J.; Schembri, M.; De Genst, E.; Cools, L.; Wuhrer, M.; Hung, C.-S.; Pinkner, J.; Slattegård, R.; Zavialov, R.; Choudhury, D.; Langermann, S.; Hultgren, S. J.; Wyns, L.; Klemm, P.; Oscarson, S.; Knight, S. D.; De Greve, H. Receptor Binding Studies Disclose a Novel Class of High-Affinity Inhibitors of the Escherichia Coli FimH Adhesin: A Novel Class of FimH High-Affinity Ligands. *Mol. Microbiol.* **2005**, *55*, 441–455.

(33) Brument, S.; Cheneau, C.; Brissonnet, Y.; Deniaud, D.; Halary, F.; Gouin, S.; Polymeric Mannosides Prevent DC-SIGN-Mediated Cell-Infection by Cytomegalovirus. *Org. Biomol. Chem.* **2017**, *15*, 7660–7671.

(34) Dam, T. K.; Oscarson, S.; Roy, R.; Das, S. K.; Pagé, D.; Macaluso, F.; Brewer, C. F. Thermodynamic, Kinetic, and Electron Microscopy Studies of Concanavalin A and Dioclea Grandiflora Lectin Cross-Linked with Synthetic Divalent Carbohydrates. *J. Biol. Chem.* **2005**, *280*, 8640–8646.

(35) Pifferi, C.; Goyard, D.; Gillon, E.; Imberty, A.; Renaudet, O. Synthesis of Mannosylated Glycodendrimers and Evaluation against Bc2L-A Lectin from Burkholderia Cenocepacia. *ChemPlusChem* **2017**, *82*, 390–398.

(36) Mydock-McGrane, L. K.; Hannan, T. J.; Janetka, J. W. Rational Design Strategies for FimH Antagonists: New Drugs on the Horizon for Urinary Tract Infection and Crohn's Disease. *Expert Opin. Drug Discov.* **2017**, *12*, 711–731.

(37) Gouin, S. G. Repurposing *Escherichia Coli* Antiadhesives in Crohn's Disease. *Future Med. Chem.* **2016**, *8*, 1903–1906.

(38) Klein, T.; Abgottspon, D.; Wittwer, M.; Rabbani, S.; Herold, J.; Jiang, X.; Kleeb, S.; Lüthi, C.; Scharenberg, M.; Bezençon, J.; Gubler, E.; Pang, L.; Smiesko, M.; Cutting, B.; Schwardt, O.; Ernst, B. FimH Antagonists for the Oral Treatment of Urinary Tract Infections: From Design and Synthesis to in Vitro and in Vivo Evaluation. *J. Med. Chem.* **2010**, *53*, 8627–8641.

(39) Cusumano, C. K.; Pinkner, J. S.; Han, Z.; Greene, S. E.; Ford, B. A.; Crowley, J. R.; Henderson, J. P.; Janetka, J. W.; Hultgren, S. J. Treatment and Prevention of Urinary Tract Infection with Orally Active FimH Inhibitors. *Sci. Transl. Med.* **2011**, *3*, 109ra115.

(40) Sivignon, A.; Yan, X.; Dorta, D. A.; Bonnet, R.; Bouckaert, J.; Fleury, E.; Bernard, J.; Gouin, S. G.; Darfeuille-Michaud, A.; Barnich, N. Development of Heptylmannoside-Based Glycoconjugate Antiadhesive Compounds against Adherent-Invasive Escherichia Coli Bacteria Associated with Crohn's Disease. *mBio* **2015**, *6*, e01298-15.

(41) Yang, H.; Mirsepasi-Lauridsen, H. C.; Struve, C.; Allaire, J. M.; Sivignon, A.; Vogl, W.; Bosman, E. S.; Ma, C.; Fotovati, A.; Reid, G. S.; Li, X.; Petersen, A. M.; Gouin, S. G.; Barnich, N.; Jacobson, K.; Yu, H. B.; Krogfelt, K. A.; Vallance, B. A. Ulcerative Colitis-Associated E. Coli Pathobionts Potentiate Colitis in Susceptible Hosts. *Gut Microbes* **2020**, *12*, 1847976.

(42) Cecioni, S.; Imberty, A.; Vidal, S. Glycomimetics versus Multivalent Glycoconjugates for the Design of High Affinity Lectin Ligands. *Chem. Rev.* **2015**, *115*, 525–561.

(43) Porkolab, V.; Chabrol, E.; Varga, N.; Ordanini, S.; Sutkevičiūtė, I.; Thépaut, M.; García-Jiménez, M. J.; Girard, E.; Nieto, P. M.; Bernardi, A.; Fieschi, F. Rational-Differential Design of Highly Specific Glycomimetic Ligands: Targeting DC-SIGN and Excluding Langerin Recognition. *ACS Chem. Biol.* **2018**, *13*, 600–608.

(44) Landemarre, L.; Duverger, E. In *Glycosylation Engineering of Biopharmaceuticals: Methods and Protocols, Methods in Molecular Biology*; Beck, A. Eds; Humana Press, Totowa, NJ, 2013; vol 988; pp. 221–226.

(45) Cauwel, M.; Sivignon, A.; Bridot, C.; Nongbe, M.-C.; Deniaud, D.; Roubinet, B.; Landemarre, L.; Felpin, F.-X.; Bouckaert, J.; Barnich N.; Gouin, S. Heptylmannose-functionalized cellulose for the binding and specific detection of pathogenic E.coli. *Chem. Commun.* **2019**, *55*, 10158–10161.

(46) Brissonnet, Y.; Assailly, C.; Saumonneau, A.; Bouckaert, J.; Maillasson, M.; Petitot, C.; Roubinet, B.; Didak, B.; Landemarre, L.; Bridot, C.; Blossey, R.; Deniaud, D.; Yan, X.; Bernard, J.; Tellier, C.; Grandjean, C.; Daligault, F.; Gouin, S. G. Multivalent Thiosialosides and Their Synergistic Interaction with Pathogenic Sialidases. *Chem. – Eur. J.* **2019**, *25*, 2358–2365.

(47) Dejmek, M.; Hřebabecký, H.; Šála, M.; Dračínský, M.; Nencka, R. Microwave-Assisted Solvent-Free Diels–Alder Reaction. *Synthesis* **2011**, *24*, 4077–4083.

(48) Miyasako, N.; Matsuoka, S.-I.; Suzuki, M. Ring-Opening Metathesis Polymerization of *endo*- and *exo*-Norbornene Lactones. *Macromol. Rapid. Commun.* **2021**, *42*, 2000326.

(49) Robertson, I. D.; Pruitt, E. L.; Moore, S. Frontal Ring-Opening Metathesis Polymerization of Exo-Dicyclopentadiene for Low Catalyst Loadings. *ACS Macro Lett.* **2016**, *5*, 593–596.

(50) Hyatt, M. G.; Walsh, D. J.; Lord, R. L.; Andino Martinez, J. G.; Guironnet, D. Mechanistic and Kinetic Studies of the Ring Opening Metathesis Polymerization of Norbornenyl Monomers by a Grubbs Third Generation Catalyst. *J. Am. Chem. Soc.* **2019**, 141, 17918–17925.

(51) Montembault, V.; Desbrosses, J.; Campistron, I.; Reyx, D. Ring-opening metathesis polymerization of 2-(*S*)-(–)-*endo*-D-pantolacton-*O*-yl norbornene-2-carboxylate using a classical ROMP catalyst. Synthesis and characterization of optically active poly(norbornene-2-carboxylic acid). *Macromol. Chem. Phys*. **2000**, 201, 973–979.

(52) Keitz, B. K.; Fedorov, A.; Grubbs, R. H. Cis-Selective Ring-Opening Metathesis Polymerization with Ruthenium Catalysts. *J. Am. Chem. Soc.* **2012**, *134*, 2040–2043.

(53) Buck, M.E.; Lynn, D.M. Azlactone-functionalized polymers as reactive platforms for the design of advanced materials: Progress in the last ten years. *Polym. Chem.* **2012**, *3*, 66–80.

(54) Ho, H. T.; Levere, M. E.; Fournier, D.; Montembault, V.; Pascual, S.; Fontaine, L. Introducing the Azlactone Functionality into Polymers through Controlled Radical Polymerization: Strategies and Recent Developments. *Aust. J. Chem.* **2012**, 65, 970–977.

(55) Fisk, J. S.; Mosey, R. A.; Tepe, J. J. The diverse chemistry of oxazol-5-(4*H*)-ones. *Chem. Soc. Rev.* **2007**, *36*, 1432–1440.

(56) Cauwel, M.; Sivignon, A.; Bridot, C.; Nongbe, M. C.; Deniaud, D.; Roubinet, B.; Landemarre, L.; Felpin F.-X.; Bouckaert, J.; Barnich, N.; Gouin, S. S. Heptylmannose-functionalized cellulose for the binding and specific detection of pathogenic *E.Coli*. *Chem. Commun.* **2019**, *55*, 10158–10161.

(57) Krammer, E.-M.; Bridot, C.; Serna, S.; Echeverria, B.; Semwal, S.; Roubinet, B.; van Noort, K.; Wilbers, R. H. P.; Bourenkov, G.; de Ruyck, J.; Landemarre, L.; Reichardt, N.; Bouckaert, J. Structural insights into a cooperative switch between one and two FimH bacterial adhesins binding pauci-and high-mannose type glycan receptors. *J. Biol. Chem.* **2023**, *299*, 104627.

(58) Lameignere, E.; Malinovská, L.; Sláviková, M.; Duchaud, E.; Mitchell, E. P.; Varrot, A.; Šedo, O.; Imberty, A.; Wimmerová, M. Structural Basis for Mannose Recognition by a Lectin from Opportunistic Bacteria Burkholderia Cenocepacia. *Biochem. J.* **2008**, *411*, 307–318.

(59) Wellens, A.; Garofalo, C.; Nguyen, H.; Gerven, N. V.; Slättegård, R.; Hernalsteens, J.-P.; Wyns, L.; Oscarson, S.; Greve, H. D.; Hultgren, S.; Bouckaert, J. Intervening with Urinary Tract Infections Using Anti-Adhesives Based on the Crystal Structure of the FimH–Oligomannose-3 Complex. *PLOS ONE* **2008**, *3*, e2040.

(60) Ashton, P. R.; Hounsell, E. F.; Jayaraman, N.; Nilsen, T. M.; Spencer, N.; Stoddart, J. F.; Young, M. Synthesis and Biological Evaluation of α-D-Mannopyranoside-Containing Dendrimers. *J. Org. Chem.* **1998**, *63*, 3429–3437.

For Table of Contents Only